Proposal for a Radio Astronomical Search for Extremely High Energy Cosmic Ray Interactions in the Lunar Regolith

David Saltzberg

Department of Physics & Astronomy
UCLA, Los Angeles, California.

Peter Gorham, Kurt Liewer, and Charles Naudet

Jet Propulsion Laboratory

ABSTRACT

We propose to use the 70 m Goldstone antenna (Deep Space Station 14) to begin a new radio astronomical search for ultra-short electromagnetic pulses that are expected to originate from particle cascades induced by extremely high energy cosmic rays and neutrinos, which interact and shower within the lunar regolith. We have completed initial studies of the feasibility of this technique, and we now propose to acquire signficantly more data which will push the sensitivity into regions that have not yet been explored with any previous detection method. We believe that the Deep Space Network facilities provide unique capabilities for this research which cannot be easily duplicated at present with any existing national facility. The method is expected to be fundamentally limited only by total integration time. At present we can analyze data at a rate equivalent to about 2 full transit passes (8-12 hrs of net integration) of the moon per month. We can make use of passes as short as 6 hrs of moon exposure. Thus we request an allocation of time commensurate with these levels, with no schedule constraints other than that the moon be visible for at least 6 hrs of the scheduled pass.

1. Scientific Motivation

Detection and characterization of extremely high energy (EHE) cosmic rays and neutrinos is expected to play an important diagnostic role in understanding the radiative kinematics of a number of cosmologically significant phenomena. Active Galactic Nuclei (AGN) may be copious producers of such particles via hadronic interactions of material energized by Fermi acceleration mechanisms at the predicted accretion shock near the central black hole. Cosmic gamma-ray bursts are expected to produce both cosmic rays and neutrinos through rapid shock acceleration during the burst and its gamma-ray afterglow. EHE cosmic rays themselves interact with a $\sim$ 10 Mpc mean free path with cosmic background photons to produce other EHE neutrinos. More exotic mechanisms such as topological defects or cosmic strings will also lead to EHE neutrino production.

The detection of EHE neutrinos is aparticularly enigmatic problem. The presence of EHE cosmic ray nuclei virtually guarantees that neutrinos should be present with even higher flux levels; yet because of their extremely low interaction cross–sections, these particles have to date escaped detection. Earth-based observatories for EHE neutrinos can only achieve adequate sensitivity by instrumenting a huge target mass. Optical Cherenkov detectors such as AMANDA and the European initiatives will in the next few years begin approaching the necessary sensitivity to detect cosmic neutrinos in the 10^{12-15} eV range. However, the EHE ($\geq 10^{18}$ eV) regime is a much more difficult problem, and none of the existing instruments appear to have capability to address it. The required volume of water or ice to detect the extremely low flux densities at $\geq 10^{18}$ eV is in range of hundreds of cubic km per year of operation.

One proposed approach to this is to use detectors in the radio regime, sensing at large distances the emission of coherent radio Cherenkov radiation from the excess charge that develops in a EHE particle cascade. This method was first suggested by Askaryan (1962, 1965), and elaborated on by Dagkesamanskii & Zheleznykh (1989), whose work motivated one prior EHE neutrino search looking for radio emission from cascades in the lunar regolith which reported a null result in 10 hours of livetime (Hankins, Ekers, & O'Sullivan 1996).

In this approach, the detector consists of a ground-based antenna and a target volume given by the several meter-thick surface layer of the lunar regolith that is within the solid angle of the telescope's primary beam pattern[1]. A primary neutrino or cosmic ray propagating near the lunar surface interacts with a nucleus and initiates a cascade of charged particles. As it reaches its maximum, the cascade, which is composed by this time primarily of electron-positron pairs, begins to lose its initial charge neutrality through annihilation of positrons, delta-ray production, and compton scattering of electrons in the material. The net excess negative charge, propagating at the speed of light in a small disk with transverse dimensions of a few cm over a distance of 5–10 m, then produces a highly linearly–polarized electromagnetic pulse which is detected in the far–field at earth. Since the beam of a 70 m antenna at S-band covers a fair fraction of the 2×10^7 km^2 visible half of the lunar surface, the potential target volume can be tens of thousands of cubic kilometers–far more than anything achievable in a ground-based installation.

1.1. Emission Mechanisms.

Because of the extreme energies involved, direct accelerator measurements of the relevant radio emission processes cannot be performed. We must instead rely on simulation of the emission, and on related measurements of pulsed electron beams which can mimic some of the characteristics expected from the cascades. Fortunately there is a growing body of such work which supports the validity of the proposed approach.

Recent work on modeling of coherent Cherenkov radio emission mechanisms in ice (Zas, Halzen & Stanev 1992) has provided detailed simulations the emission of radio Cherenkov radiation for cascade energies up to $\sim 10^{16}$ eV. This initial work was later extended by Alvarez-Muñiz & Zas (1997, 1998) in energy up to 10^{20} eV, including corrections as the Landau–Pomeranchuk–Migdal (LPM) effect. Related

---

[1]At 2 GHz, the attenuation length of radio waves propagating in the regolith is 3–5 m

work by Alvarez–Muñiz & Zas (1996) considered the effects of the lunar regolith density and surface geometry on the propagation of the pulsed emission.

The conclusions of all of these modeling efforts have only strengthened the consensus that lunar cascades should produce measurable pulsed emission at cm wavelengths. In fact, the radio emission is expected to peak at $\sim 1-2$ GHz, and extend up to ~ 10 GHz before loss of coherence begins to strongly attenuate the signal. Thus the emission is well-matched to the receiving capabilities of many radio telescopes in the 2–20 cm-wavelength region.

The flux densities expected from such a cascade can be estimated by considering the power emitted by a group of charged particles via the coherent Cherenkov process, as described by the Frank–Tamm equation:

$$\frac{d^2W}{d\nu dl} = (Ne)^2 \left[\frac{4\pi^2\hbar\alpha}{c}\right]\left[1-\frac{1}{\beta^2 n^2}\right] \tag{1}$$

where l is the shower tracklength, ν is the frequency of the radiation, N is the number of particles of charge e, $\alpha = \frac{1}{137}$ is the fine structure constant, β is the velocity of the group of particles, and $n \sim 2.8$ is the index of refraction of the medium (in this case the regolith).

The number of charged leptons around cascade maximum is given to a good approximation by expressing the cascade energy in GeV; thus a 10^{20} eV shower will cascade down to of order 10^{11} electron positron pairs near the cascade maximum. The excess in electrons will be about 20% of this; thus $N \approx 2 \times 10^{10}$, with mean energy of order 100 MeV (thus $\beta = 1$). Accounting for the angular dependence of the Cherenkov emission, which comes out as a cone at 56° from the track direction, one can parameterize the peak flux density in the cm wavelength regime as (Dagkesamansky & Zheleznykh 1989):

$$S_\nu \approx 3\times 10^{-23}\left[\frac{\nu}{1\ \mathrm{GHz}}\right]\left[\frac{E}{10^{20}\ \mathrm{eV}}\right]^2 \quad \mathrm{W\ m^{-2}\ Hz^{-1}} \tag{2}$$

where ν is the radio frequency and E is the cascade energy. The linear increase with radio frequency is actually expected to turn over slowly around 1.5-2 GHz due to partial loss of coherence. However, based on these results we expect a 10^{20} eV cascade to produce a pulse of order 5000 Jy at S-band.[2]

Figure 1 plots the expected RF spectrum (upper) and pulse shape (lower) from a 10^{20} eV lunar cascade as received at Earth, including the effects of the ionosphere (total electron content 10^{17} cm^{-2}). At high frequencies (≥ 2 GHz) the effects of the ionosphere are negligible and the pulse duration is of order 1 ns.

1.1.1. Relevant LINAC measurements.

There are now laboratory measurements of coherent Cherenkov and transition radiation from electron bunches in electron linear accelerators (Ohkuma et al 1991; Shibata et al 1991; Takahashi et al 1994).

[2]Such large values for the flux density reflect the fact that the emission occurs over an extremely short time.

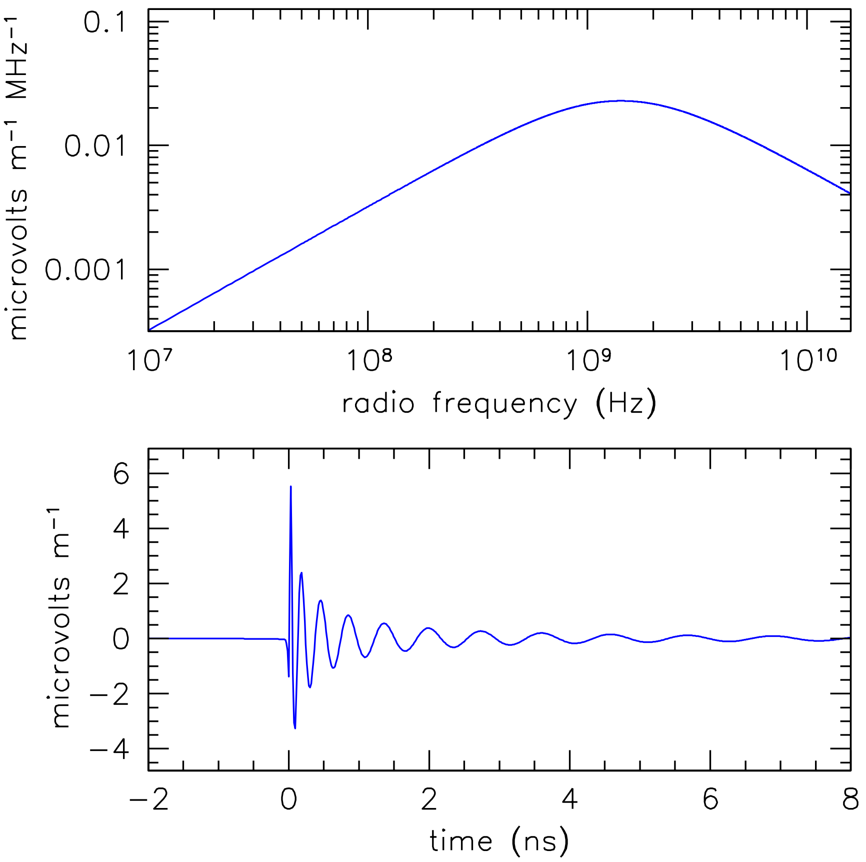

Fig. 1.— Expected spectrum and shape for a 10^{20} eV lunar cascade radio pulse,including typical ionospheric dispersion. Based on models of Alvarez-Muñiz & Zas 1996, 1997, 1998.

These experiments confirm the quadratic dependence of output power on electron number, and also verify a number of important predictions relevant to the emission process, such as: formation zone effects, finite track–length effects, and interference behavior related to the coherence of the emitted waves. Thus we can begin to have some confidence that predictions of lunar cascade emission should be taken seriously.

2. Proof-of-Concept Experimental Setup

To investigate the possibility of detecting pulsed lunar cascade emission, we have completed an initial series of single and dual antenna measurements using the NASA Goldstone Deep Space Stations DSS14 and DSS13. Since the expected pulse from a cascade is of order 1 ns in duration, standard continuum radio astronomy instrumentation is inadequate, and we have developed our own time–domain data acquistion system, which directly samples the broadband downconverted signals. This type of time–domain system, which operates directly on the band-limited IF voltages from the front-end amplifiers, is unusal for radio astronomical applications. It is perhaps most akin to single–pulse detection in pulsar studies, but the time scales of interest of order a thousand times shorter than the most rapid pulsar sampling.

Our experimental setup for single–antenna measurements involved a trigger system which required a ≥ 5 ns time overlap of fixed–width (10-20 ns) logic pulses generated directly from the S–band left (LCP) and right (RCP) circular polarization IF bandpass voltages and a fast discriminator. Since Cherenkov emission is 100% linearly polarized, a pulse of Cherenkov radiation will produce an equal amplitude voltage pulse in both LCP and RCP. This type of coincidence is very effective at rejecting interference from microwave telemetry systems (such as those on earth-orbiting satellites) since these are almost universally circularly polarized.

However, such a coincidence is sensitive to impulsive interference, such as that generated by any short-path high-voltage arcing phenomena, which are also typically linearly polarized. Thus an enhancement to the trigger was developed which utilized a second receiver and the L-band feed horn. When DSS 14 is used at S-band, the L-band feed views a region of the sky about 0.5° away. Tests of the off-axis L-band response to an on–axis S-band source have shown it to be negligible. Local terrestrial impulsive interference couples to the feed horns either by "flashing" across the sky, or scattering directly from antenna structure (such as the subreflector). Such interference also tends to be steep-spectrum, falling off quickly at higher frequencies.

We have found in practice that, by using the L-band signal as a veto, we can virtually eliminate any triggers from terrestrial interference. This was tested several times at DSS 14, including once under extreme conditions when the trigger rate (for $> 4.5\sigma$ pulses in both polarizations) was 1.5 kHz without the veto. With the veto turned on, the rate of interference triggers decreased to ≤ 0.01 Hz, a factor of $\geq 10^5$ rejection. Such conditions are atypical (average rates of interference triggers are one every few minutes or less), but demonstrate clearly the effectiveness of this method.

Once a trigger is generated, the IF voltage time series for each of the signals present: S-band LCP, S-band RCP, and L-band LCP (veto), are sampled at 1 GHz using a Tektronix TDS784 digital oscilloscope, then read out to computer. Figure 2 shows an example of a single trigger. The top pane shows the instantaneous power levels in each of the two S-band IFs. The power is normalized to the mean thermal noise power in each case. The pane to right of each window shows the statistics of the power distribution over a period of $\pm 2.5\mu$s around the trigger, with the expected thermal distribution (exponential in power) plotted as a fitted line on each graph.

The effects of the bandpass of each IF are evident in the trigger time series: the LCP, which had a 100 MHz bandpass, has the faster risetime and pulse width compared to RCP, with a 40 MHz bandpass. The middle window shows the veto signal, which in this case indicates that the trigger was due to RF interference which was not vetoed. The presence of the coincident L-band pulse with the S-band pulses, and the noisy character of the S-band data shows clearly the RFI nature of this trigger. The final window at the bottom shows the sampled data arriving from DSS13, offset in time to the window corresponding to the

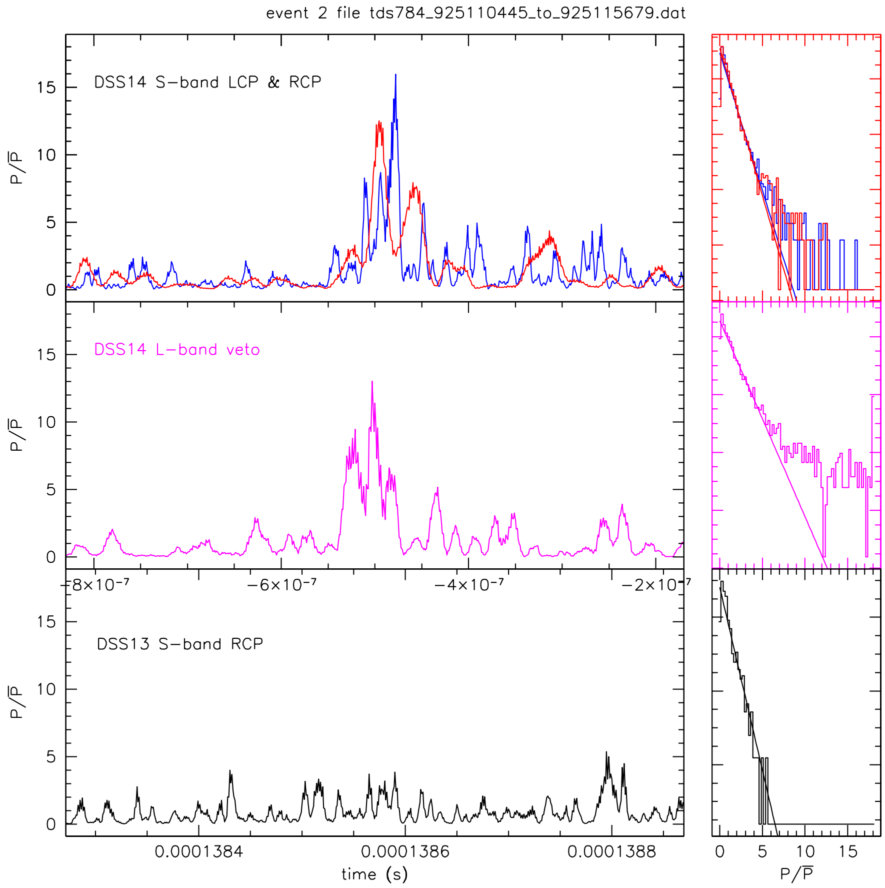

Fig. 2.— An example of a RF interference trigger. Such triggers are relatively rare and easily distinguished by the presence of the noise in the L-band veto signal.

correct delay from the moon.[3]

Post–analysis of the recorded triggers requires that they are:

1. Band-limited in width, consistent with expectations that the cascade pulses are ~ 1ns in duration;

2. Not significantly offset in time, or greatly different in amplitude in RCP and LCP;

3. Without any significant counterpart in the L-band recorded signal, indicating that they are not likely to be terrestrial in origin;

[3]The "clock offset" component of the delay for the moon is determined using interferometric correlation of a bright quasar with the present system for a 15 microsecond integration. Subtracting off the geometric delay for the quasar position gives the fixed component. The moon's variable geometric delay is then given by the antenna tracking software which has been verified by boresighting. Delays can be estimated to an accuracy of several ns with this approach.

4. Of sufficient amplitude in each polarization that they are statistically very unlikely from random thermal noise fluctuations.

5. In the case of the dual antenna system, an additional criterion is included with those above: A band-limited pulse must appear in the DSS 13 IF data coincident in the time window that is consistent with the geometric delay to the surface of the Moon viewed by the two antennas.

In practice the width of the window for DSS13 overlap must be of order $B\Theta_m c^{-1} \approx \pm 290$ns (where B is the baseline and Θ_m is the angular size of the Moon) to account for cascades at any point on the Moon's surface.

3. Initial Results

In our proof-of-concept tests, the hardware trigger was as loose as the data collection system could tolerate, giving trigger rates of 0.1 Hz for the single– and 0.01 Hz for the dual–antenna operation. Since the great majority of these triggers were random thermal noise coincident pulses of the two polarizations our post-processing of the data involved setting a threshold which was well beyond any possibility of random noise coincidence. Thus we required the signals from the 70m antenna (DSS 14) to exceed the 6σ level in both LCP and RCP, along with an additional requirement of $\geq 4\sigma$ from the DSS 13 signal.

These requirements can be transformed into an energy threshold for the system, based on the cascade simulations noted above and the standard Dicke equation for radio antenna sensitivity:

$$\Delta S = \frac{2kT_{sys}}{A_{eff}(\Delta t \Delta\nu)^{0.5}} \quad . \tag{3}$$

The mean thermal noise power for our system is ~ 150 Jy, giving a post-analysis 6σ threshold of about 3000 Jy.[4] This in turn corresponds to the flux density expected from a $\sim 3 \times 10^{19}$ eV cascade. Because of the inelastic nature of the particle collisions at these energies, we estimate our neutrino energy threshold to be 8×10^{19} eV, with the peak sensitivity (weighted by effective volume and an E^{-2} spectrum) at an energy about a factor of 4 higher than this.

In our initial test of these methods, we have observed the Moon for a total of 11.9 hrs. Of the ~ 300 (in 8 hrs) dual antenna and ~ 1100 (in 4 hrs) single antenna triggers, none matched all of the criteria above[5]. We have thus established the necessary background rejection to achieve adequate sensitivity to detect a signal if it present, given the necessary livetime.

---

[4]Note that the equivalent power level corresponding to the 6σ Gaussian significance is about 20 times the noise power.

[5]In both the single–and dual–antenna case, the vast majority of the triggers are simple thermal noise coincidences near the hardware threshold of 4.5σ in each polarization. The remaining triggers are obvious RF interference where the veto pulse level fell below the more conservative ($\geq 5\sigma$) veto threshold, but is still clearly present in the sampled L-band IF data.

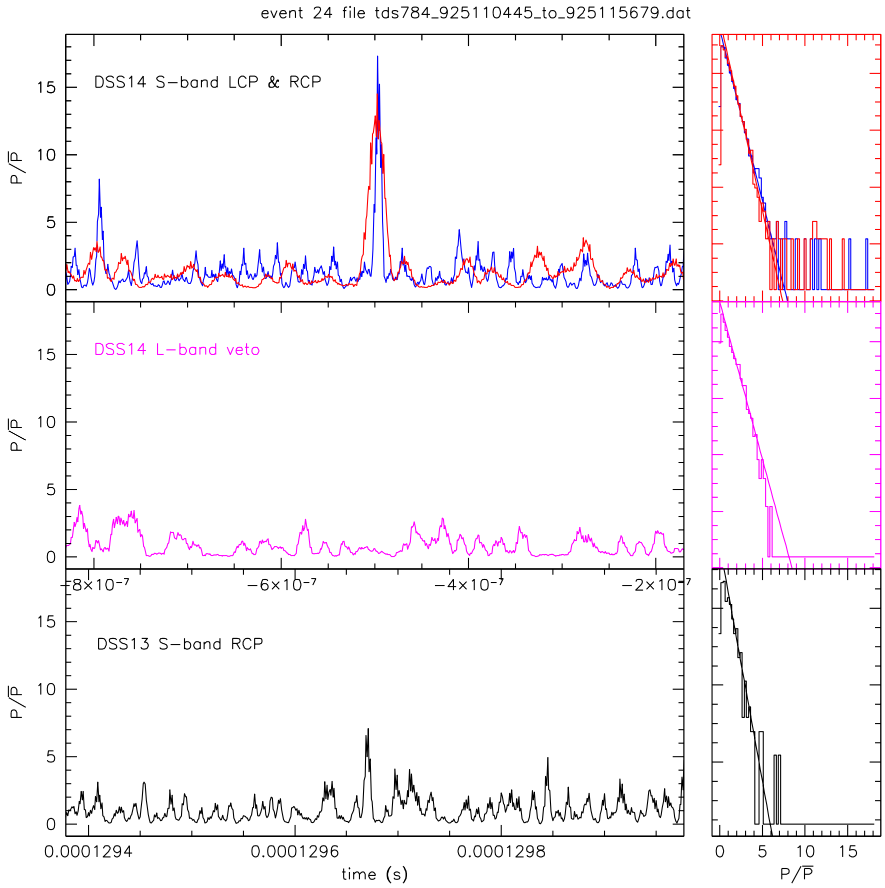

Fig. 3.— An event which display many of the characteristics of a possible signal, but is not yet statistically signficant.

This initial analysis is necessarily conservative, but we expect our sensitivity to improve as the analysis methods are refined. In Figure 3 we show an event which nearly satisfies the criteria mentioned above, but falls just below our present threshold. Here the pulses are band-limited in S-band, there is no L-band signal present, and a corresponding pulse appears at DSS13 which is consistent with the DSS14 amplitude. We are presently assessing the statistical significance of events such as these. While such events may not yet be individually statistically significant, an ensemble of them obtained over a larger sequence of observations may still provide the evidence that we need to verify the presence of a particle flux.

3.1. Limits on EHE neutrinos.

To indicate the potential sensitivity of this method, we have estimated the flux limits corresponding to our initial 12 hr livetime. Figure 4 plots the predicted fluxes of EHE neutrinos from a number of models including AGN production (Mannheim 1996, M) gamma-ray bursts (Bahcall & Waxman 1999, BW), EHE cosmic-ray interactions (Hill & Schramm 1985, HS), and topological defects (TDs; Yoshida et al 1997, YTD; Bhattacharjee et al 1992, BTD; Sigl et al 1996, STD). Also plotted are limits from about 70 days of Fly's Eye livetime (Baltrusaitas et al 1985).

Our initial 90% CL limit, based only on our proof–of–concept livetime, is shown plotted with inverted triangles (cf. Gorham, Liewer, & Naudet 1999). We find that, even with our limited total integration time to date, we have already set the only limit in this energy regime, and have nearly achieved a sensitivity sufficient to constrain some of the theoretical flux predictions for EHE neutrinos.[6]

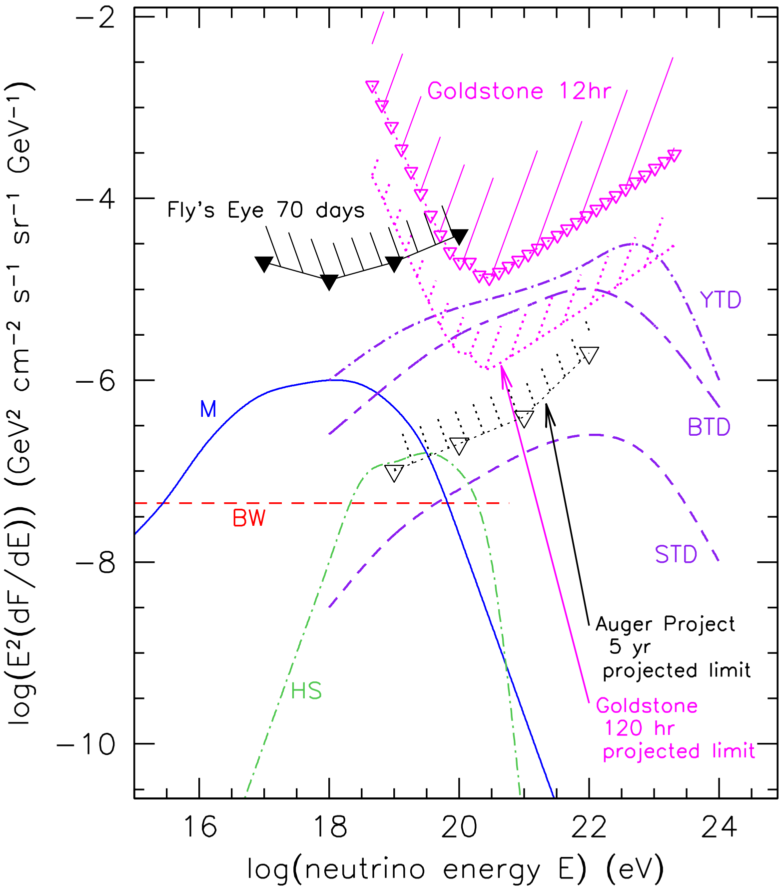

Fig. 4.— Predictions & limits for EHE neutrinos (details in text).

[6]The behavior of our differential limit was determined by semi–analytic modeling of the effects of the antenna beam response, the emission geometry, and RF attenuation of the regolith.

4. Requested & contributed resources.

To provide the motiviation for our time allocation request, we refer to Fig. 4 again to indicate the scientific justification for the requested time. Plotted in Fig. 2 are projected 5 yr livetime limits for the planned Auger Project (Capelle et al 1998) which is due to begin construction early in the next millenium. For comparison we also plot projected Goldstone sensitivity limits for a factor of 10 greater livetime (120 hrs) than we have achieved in our test observations to date. This level of livetime corresponds approximately to our requested time in this proposal for the next calendar year, accounting for an observing efficiency (equipment failures, schedule conflicts, etc.) of 70-80%. The sensitivity that we can achieve given this additional observing time will potentially detect EHE neutrinos at a significant flux level if either of the two models shown for topological defect sources are correct.

It is also quite striking that even this near term committment of resources at Goldstone can potentially come within a factor of four of the projected 5 year livetime sensitivity of the Auger project, a very large scale ground-based cosmic-ray detector with an expected cost of order $50M. Accounting for the Auger project startup and observing efficiency, this level of their livetime may in fact not be achieved for at least another decade of real time. Although the radiodetection method cannot provide the degree of particle identification and angular resolution that the Auger array will have, it has a clear potential to achieve a greater sensitivity, and at a much earlier time, if the expectations of the technique are born out in our continued observations.

We therefore request 1–2 passes per month of DSS 14 time, which individually yield at least 6 hrs of visibility of the moon. We would prefer a single pass per month of 10 hrs or more, since this would reduce our observing overhead; however we wish to be flexible in our scheduling. We have only one other schedule constraint: that is, we propose to make dual antenna observations whenever possible, and thus require that time at the dedicated research antenna DSS 13 be co-allocated to correspond to the scheduled time at DSS 14.

4.1. Uniqueness of Goldstone Capabilities.

The facilities afforded by the Goldstone Tracking Station have provided certain unique capabilities for this experiment which could not be easily duplicated at US NRAO facilities. In this section we highlight several of these.

4.1.1. L-band Veto Capability.

One of the most important facets of our experiment in comparison to the only predecessor experiment at the Parkes 64 m (Hankins et al 1996) is our ability to configure an effective real-time veto for RF interference. This capability is made possible because of the front-end and feed configuration of DSS 14, which allows us to have simultaneous access to broad-band signals from both L and S-band, while both feeds view the sky. Since the L-band feed is still reasonably efficient even when the antenna if focussed for S-band, and because it views a region of sky near the source, it is extremely effective as a flag for the rpesence of impulsive RFI, as we have discussed above. This capability is simply not easily attainable at most radio astronomical observatories, because it does not represent a configuration that would have any normal benefit to typical continuum or spectral line observations.

4.1.2. DSS 13 Real-time Link.

Even with real–time veto capability, low–level RFI could produce spurious triggers which might be interpreted as lunar pulses in any single–antenna system. Even a dual antenna system with too short of a baseline might not completely reject such spurious events. Thus we believe that dual or multiple antenna capability will be critical to the success of any search of this type. However, over too long of a baseline, the lunar pulses may become decorrelated, since the Cherenkov emission is of order 1° or less in angular width. This means that at separations longer than a few hundred km, the common-mode detection of lunar pulses could become less efficient. In fact, the ideal separation of antennas is much less than this, and is determined by the requirement that RFI is not common-mode at the two stations.

Such considerations, combined with the desirability of a realtime link, leads us to see the DSS 14–DSS 13 pair as a very important attribute of Goldstone facilities. Ideally, a VLA-like configuration with many antennas grouped over a 30 km diameter area would give the best background rejection, but a committment of this large a set of resources would be difficult to achieve at this stage, and the VLA antenna size is much smaller than the 70 m. It appears that the combination of a 70 m class antenna and a realtime link to a system like DSS 13, with its very broadband (≥ 150 MHz) S-band HEMT front end is a capability that is unique for our application.

4.2. Outside contributions & related proposals

If this proposal is approved, D. Saltzberg intends to provide equipment funding at the level of $20K to support acquiring dedicated data acquisition hardware to replace a portion of the equipment which has been rented up till now. This equipment is intended to reside in an electronics rack at DSS 14 if a rack location can be made available.

In addition to this support, we are proposing additional funding for UCLA graduate student support (through NSF). We are also preparing a JPL Director's Discretionary Research Fund (DRDF) proposal for addition funds to improve the data acquisition system. Both of these proposals are contingent on approval of this request.

We note here that our effort is not likely to be without international competition for long. A European initiative to begin a similar program is in progress, although at a more nascent level than ours at present.

4.3. Organization of Effort

In a number of ways the time–domain techniques that we are using for pulse detection are very similar to the methods used in high energy particle physics detectors. D. Saltzberg has an extensive background in detector development for such applications and will provide significant expertise and equipment resources from high energy physics equipment under his control at UCLA. He also has strong current research interests in particle astrophysics and is an active member of the expanding particle astrophysics team at UCLA.

P. Gorham has a background in both traditional radio astronomical research, including VLA radio imaging and extensive pulsar observations at the Arecibo 300 m antenna; and in particle astrophysics, including TeV gamma-ray observations and previous searches for high energy cosmic neutrinos. C. Naudet and K. Liewer have both had many years of experience using DSN antennas and the associated radio astronomical instrumentation at the DSN. They have provided essential understanding of the observing configurations and have enabled highly efficient adaptation of existing DSN resources in the execution of the initial test observations of this project.

References

Alvarez–Muñiz, J., & Zas, E., 1997, Phys. Lett. B, 411, 218; also 1998, LANL preprint astro-ph 9806098.

Alvarez–Muñiz, J., & Zas, E., 1996, Proc. XXVth ICRC, ed. M.S. Potgeiter, et al. vol. 7, 309.

Askaryan, G.A.,1962, JETP 14, 441; also 1965, JETP 21, 658.

Bahcall, J.N., and Waxman, E., 1999, LANL preprint astro-ph 9902383.

Baltrusaitas, R.M., Cassiday, G.L., Elbert, J.W., et al 1985, Phys Rev D 31, 2192.

Bhattacharjee, P., Hill, C.T., & Schramm, 1992, D.N, PRL 69, 567.

Capelle, K.S., Cronin, J.W., Parente, G., & Zas, E., 1998, Astropart. Phys. 8, 321.

Dagkesamanskii, R.D., & Zheleznyk, I.M., 1989, JETP 50, 233.

Gorham, P.W., Liewer, K.M, and Naudet, C.J., 1999, Proc. 26th ICRC, in press.

Hankins, T.H., Ekers, R.D. & O'Sullivan, J.D. 1996, MNRAS 283, 1027.

Hill, C.T., & Schramm, D.N., 1985, Phys Rev D 31, 564.

Mannheim, K., 1996, Astropart. Phys 3, 295.

Ohkuma, J., Okuda, S., & Tsumori, K., 1991, PRL 66, 1967.

Shibata, Y. , Ishi, K., Takahashi, T., et al, 1991, Phys Rev A 44, 3449.

Takahashi, T, Kanai, T., Shibata, Y., et al, 1994, Phys Rev E 50, 4041.

Yoshida, S., Dai, H., Jui, C.C.H., & Sommers, P., 1997, ApJ 479, 547.

Zas, E., Halzen, F., & Stanev, T., 1992, Phys Rev D 45, 362.